

New Powder Metallurgical Approach to Achieve High Fatigue Strength in Ti-6Al-4V Alloy



FEI CAO, K.S. RAVI CHANDRAN, PANKAJ KUMAR, PEI SUN, Z. ZAK FANG,
and MARK KOOPMAN

Recently, manufacturing of titanium by sintering and dehydrogenation of hydride powders has generated a great deal of interest. An overarching concern regarding powder metallurgy (PM) titanium is that critical mechanical properties, especially the high-cycle fatigue strength, are lower than those of wrought titanium alloys. It is demonstrated here that PM Ti-6Al-4V alloy with mechanical properties comparable (in fatigue strength) and exceeding (in tensile properties) those of wrought Ti-6Al-4V can be produced from titanium hydride powder, through the hydrogen sintering and phase transformation process. Tensile and fatigue behavior, as well as fatigue fracture mechanisms, have been investigated under three processing conditions. It is shown that a reduction in the size of extreme-sized pores by changing the hydride particle size distribution can lead to improved fatigue strength. Further densification by pneumatic isostatic forging leads to a fatigue strength of ~550 MPa, comparable to the best of PM Ti-6Al-4V alloys prepared by other methods and approaching the fatigue strengths of wrought Ti-6Al-4V alloys. The microstructural factors that limit fatigue strength in PM titanium have been investigated, and pathways to achieve greater fatigue strengths in PM Ti-6Al-4V alloys have been identified.

DOI: 10.1007/s11661-016-3409-7

© The Minerals, Metals & Materials Society and ASM International 2016

I. INTRODUCTION

TITANIUM powder metallurgy has been pursued for many years with the goal of reducing the cost of Ti manufacturing, and obtaining near-net-shape products with reduced fabrication steps.^[1-4] Great emphasis was placed on PM manufacturing of titanium in the 1980 to 1990s, in order to successfully implement PM titanium components in aerospace applications. In these efforts, principally two approaches, the blended elemental (BE) powder approach and the pre-alloyed (PA) powder approach, have been undertaken to prepare PM titanium components. In the BE approach, titanium and other elemental component powders required to prepare an alloy of a specific composition are blended, compacted, and sintered at a sufficiently high temperature (usually in the β -phase field) to obtain the final alloy. In the PA approach, the powders of the required alloy composition are first prepared by atomization of the liquid alloy, followed by consolidation of powders by hot isostatic pressing (HIP). The PA products typically have superior mechanical properties to those of BE products due to higher density and uniformity of composition, resulting from the fully melted alloy. However, the costs of PA products are significantly

higher, for reasons that are obvious from the steps of the method. Therefore, the BE method has been the generally preferred method to prepare PM titanium alloy parts at low cost.^[5] However, the main drawback of the conventional BE PM method is the necessity to sinter in the β -phase field, which leads to a coarse colony microstructure with aligned α platelets, along with a thick layer of grain boundary α phase.^[6-8] Both of these microstructural features are detrimental to HCF strength. Since titanium alloy parts are used in fatigue critical components, especially in aerospace and potentially in automotive applications, PM process innovations that target full densification without microstructure coarsening are necessary to improve the HCF strength of PM titanium alloys. Such improvements will allow PM titanium alloys to effectively compete with wrought titanium alloys.

The wrought Ti-6Al-4V alloy microstructures show fatigue strength levels (defined as the cyclic stress amplitude at which the sample survives for 10^7 cycles) ranging from about 400 MPa to about 700 MPa.^[9] This range is generally due to the variations in processing and microstructures. Historically, the PM sintered Ti-6Al-4V alloys without any further processing have had fatigue strength levels below this range. In one of the earliest studies, Anderson *et al.*^[2] used titanium sponge fines to fabricate a PM Ti-6Al-4V alloy. The alloy had a very low fatigue endurance limit (280 MPa). In a later work, Fujita *et al.*^[1] employed sponge fines or titanium powders obtained by the hydride-dehydride process as two different starting powder forms and sintered Ti-6Al-4V samples at 1533 K (1260 °C) under vacuum for 4 hours. The samples achieved densities >99

FEI CAO and PANKAJ KUMAR, Graduate Research Assistants, K.S. RAVI CHANDRAN and Z. ZAK FANG, Professors, PEI SUN, Postdoctoral Fellow, and MARK KOOPMAN, Research Professor, are with the Department of Metallurgical Engineering, University of Utah, Salt Lake City UT 84112. Contact e-mail: ravi.chandran@utah.edu

Manuscript submitted October 12, 2015.

Article published online February 29, 2016

pct. The fatigue endurance limit was approximately 370 MPa for the specimens prepared from the sponge fines. Because it is almost impossible to eliminate all the pores by sintering, HIP was used to close the residual pores in many studies. Hagiwara *et al.*^[7] achieved an improved fatigue endurance limit (411 MPa) by applying HIP to the sintered BE compacts. The result supports the idea that reduction of porosity can lead to higher levels of fatigue strength.

Recently, a new PM process (HSPT) that involves sintering of TiH₂ powder in the β -phase field and obtaining the Ti-6Al-4V alloy by subsequent phase transformation and dehydrogenation has been introduced.^[4,10-12] The advantage of the HSPT process is that a high density and a very fine microstructure, in the as-sintered state, can be achieved at moderate sintering temperatures. The raw TiH₂ powder is also less expensive than PA titanium powders produced by the pre-alloyed rotating electrode (PREP) process or the liquid alloy atomization process. According to the (Ti-6Al-4V)-H phase diagrams developed by different authors, β phase exists above about 1073 K (800 °C) in the Ti-6Al-4V-H system, at hydrogen concentrations >10 at. pct.^[11,13-15] In the studies by Kerr and Qazi *et al.*,^[13,15] provided that there is a sufficient amount of hydrogen in β solution, the β phase was hypothesized to transform into α and hydride phase upon cooling below this temperature. Since this transformation is eutectoid in nature, a very fine microstructure resulted. Sun *et al.* illustrated that the precipitation of α/α_2 phases within β grains during isothermal holding at temperatures below the β -transus under a hydrogen atmosphere, and the eutectoid transformation of remaining β into α and hydride phase at a lower temperature, is critical for the formation of the final fine $\alpha + \beta$ microstructure.^[11,12] On this basis, in the HSPT process, the sintering of TiH₂ powder compacts is done in the β -phase field in hydrogen atmosphere and the subsequent phase transformation and dehydrogenation of the sintered Ti-6Al-4V-H alloy are performed below 1073 K (800 °C), to produce a very fine $\alpha + \beta$ Widmanstätten microstructure.^[11,13,16]

The fatigue performance of the HSPT Ti-6Al-4V alloy with such a fine microstructure is therefore quite intriguing. The objective of this work is to demonstrate that PM Ti-6Al-4V alloys with high fatigue strength levels can be obtained using this HSPT process. In light of the previous attempts to enhance the fatigue strength levels of PM titanium materials, the principal question is how much improvement in fatigue performance occurs due to porosity reduction versus microstructure refinement. To explore this, the tensile and fatigue properties of HSPT Ti-6Al-4V fabricated from two different powder size distributions were investigated in this work. The mechanisms of fatigue crack initiation were investigated by fractography. It is demonstrated that fatigue strengths that can be achieved are higher than those obtainable *via* conventional PM methods. It is shown that the fatigue performance can be improved by reducing the porosity. Additionally, comparing the present microstructure with that from other BE PM approaches, it appears that the very fine microstructure also contributes to some extent to the improved fatigue strength. The complete closure of remaining pores by the PIF process resulted in even greater improvements in fatigue strength, to levels approaching those of wrought Ti-6Al-4V alloy.

II. EXPERIMENTAL PROCEDURES

The as-received TiH₂ powders (Reading Alloys, Ametek, Robesonia, PA) had a size range of -20/+60 mesh. Figure 1(a) illustrates the shapes of the as-received powders. The powders were milled for 30 minutes and then sieved to obtain -325 or -400 mesh powders. The sieved TiH₂ powders were mixed with -400 mesh 60Al/40V master alloy powder (sieved from the -325 mesh powder provided by Reading Alloys, Ametek, Robesonia, PA). The morphology of the powders after mixing with the master alloy powder is shown in Figure 1(b). The TiH₂ particles are generally angular in shape. The particle size distributions were determined by a laser diffraction-based particle size analyzer and are

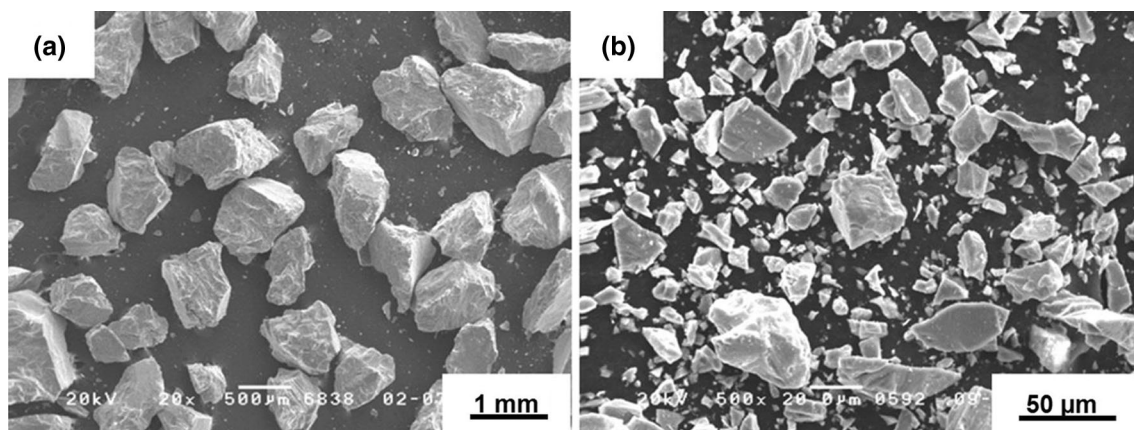


Fig. 1—Shape and size distribution of TiH₂ powder: (a) as-received -20/+60 mesh powder and (b) after blending the -325 mesh powder with the master alloy powder.

shown in Figure 2. The mean particle diameters for the –325 and –400 mesh powders were 25.3 and 20.6 μm , respectively.

Cylindrical Ti-6Al-4V bars were prepared by following the HSPT process. The details of the process are described elsewhere.^[4,10] Briefly, the process involves first cold isostatic pressing (CIP) of the mixed TiH₂ and 60Al/40V master alloy powder at 350 MPa. After CIP, the green compacts were sintered at 1473 K (1200 °C) for 4 or 8 hours in a flowing atmosphere of Ar/H₂ (50/50) mixture. The sintered samples were then phase-transformed by furnace cooling to and holding at 923 K (650 °C) for 4 hours. This was followed by dehydrogenation at 1023 K (750 °C) for 12 hours to yield a Ti-6Al-4V alloy with fine $\alpha + \beta$ microstructure. Sintered bars were pneumatic isostatic forged (PIFed) at Ametek Inc. at 1123 K (850 °C) for a short time (5 to 10 minutes). The chemical composition of the sintered Ti-6Al-4V PM alloy was determined by ICP-MS analysis. The densities of the materials were determined using the Archimedes' principle. The size distribution of the pores was determined on metallographically polished sections, using ImageJ software, over 10 mm² areas. Microstructures were examined using an SEM equipped with an EBSD detector.

Tensile properties were determined using samples prepared according to the ASTM-E8 standard and tested at a strain rate of 0.002 S⁻¹ at room temperature. Fatigue specimens having a total length of 76.2 mm were machined from sintered blanks. The test section was 6.35 mm in diameter and 12.7 mm in length. The test sections were polished using SiC paper until grade 1200, followed by finishing with 1 μm alumina suspension to

obtain surfaces free from machining damage and residual stress. Tension–tension fatigue tests were conducted under load control with a cyclic frequency of 35 Hz (sine wave), at a stress ratio ($\sigma_{\text{min}}/\sigma_{\text{max}}$) of 0.1, in a 100 kN MTS 810 testing system. The fatigue tests were conducted in laboratory air at room temperature. The wrought Ti-6Al-4V alloy specimens in mill-annealed condition were also tested in the same condition for fatigue performance comparison. Replicate tests were made until the stress-versus-fatigue-life trends were clearly revealed in the data. Fatigue fracture surfaces were examined in an SEM.

III. RESULTS AND DISCUSSION

A. Materials and Microstructures

Table I summarizes the alloy compositions obtained in the three processing conditions that were investigated in this work. The materials were prepared from –325 and –400 mesh TiH₂ powders. The choice of –325 and –400 mesh powders was made for two reasons. First, powder sizes coarser than 325 mesh resulted in densities <98 pct, and properties of such samples were deemed unlikely to be superior to those previously achieved. Secondly, any reduction of powder size less than 400 mesh, targeted to achieve improved densification during sintering, resulted in a large increase in oxygen level during the milling process, which severely reduced the tensile ductility of the sintered alloy. Hence, powder sizes coarser than –325 mesh and finer than –400 mesh were not pursued.

The compositions of Ti-6Al-4V alloys, shown in Table I, were generally within the composition range specified for a wrought Ti-6Al-4V alloy. The oxygen level, however, varied between 0.223 and 0.238 wt pct, which is slightly higher than that (0.2 wt pct) specified as a maximum for a wrought Ti-6Al-4V alloy. This difference is not expected to be significant in the context of the present work.

Microstructures of the Ti-6Al-4V alloys prepared in this work are shown in Figure 3. Figures 3(a) and (b) show optical and SEM micrographs of the alloy prepared from –325 mesh powders and sintered for 4 hours at 1473 K (1200 °C), hereafter referred to as –325 HSPT. Figures 3(c) and (d) show the microstructures of the alloy prepared from –400 mesh powders and sintered for 8 hours at 1473 K (1200 °C), hereafter referred to as –400 HSPT. Generally, the microstructures are very similar between the samples prepared from –325 mesh and –400 mesh powders. Figures 3(e) and (f) show the microstructure of the alloy after PIF of –400 HSPT samples. The prior- β grain size is essentially

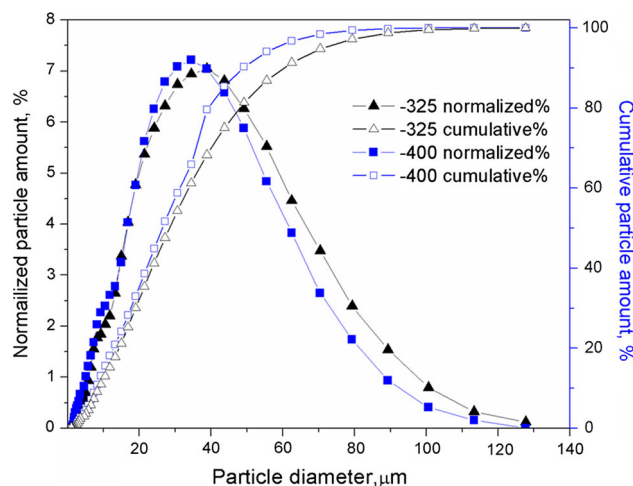


Fig. 2—Particle size distributions of mixed TiH₂ and 60Al/40V master alloy powder.

Table I. Compositions of HSPT-Processed Ti-6Al-4V Alloys in Weight Percent

Specimen	Ti	Al	V	O	H	N
–325 HSPT/4 h	—	—	—	0.238	0.000237	0.0167
–400 HSPT/8 h	bal.	5.99	3.84	0.223	0.000276	0.0175
–400 HSPT/4 h + PIF	—	—	—	0.225	0.000448	0.0176

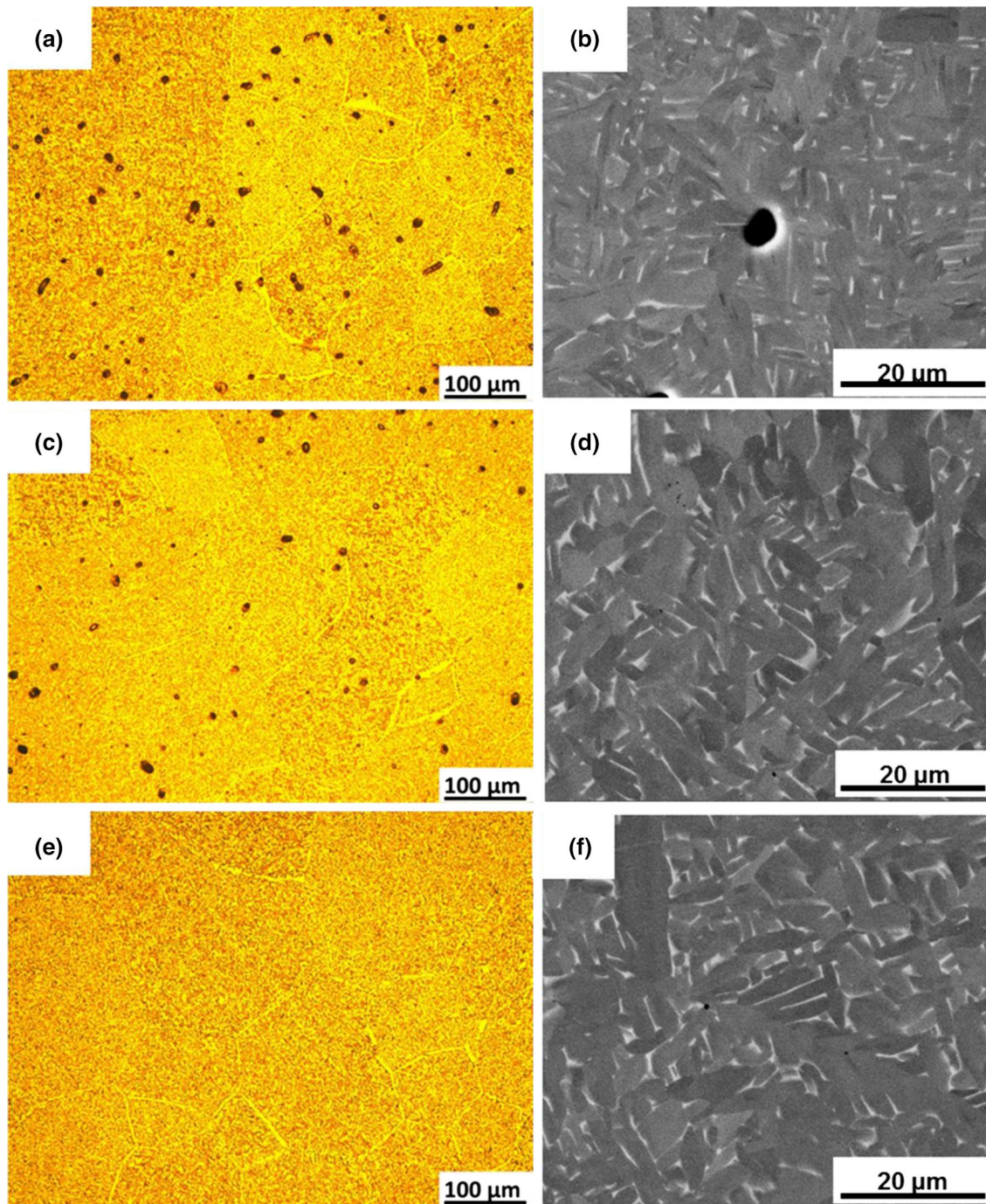


Fig. 3—Optical and SEM micrographs of Ti-6Al-4V alloys after sintering and dehydrogenation prepared with (a, b) –325 mesh powder (4 h), (c, d) –400 mesh powder (8 h), and (e, f) –400 mesh powder (4 h) followed by PIF consolidation.

equivalent to that in the as-sintered state (Figures 3(a) and (c)). However, the major change is that all the residual pores after sintering were closed by the PIF process. There were no obvious traces of the closed pores in the PIFed –400 HSPT samples.

Figure 4 shows the size distributions of the pores in the –325 HSPT and –400 HSPT samples by image analysis. Here, the pore size is characterized as the equivalent diameter of a circle that has the same area as that of an arbitrarily shaped pore in the polished

section. Pores with an area smaller than $5 \mu\text{m}^2$ were neglected by setting $5 \mu\text{m}^2$ as the threshold during image processing in ImageJ. Such small pores were found not to affect the fatigue behavior unless they were inter-connected or present as clusters. The size distributions of pores showed that the differences in porosity between the –325 HSPT and the –400 HSPT samples came from two aspects. First is that, as seen in Figure 4, the amount of small pores is greatly reduced. Secondly, the largest pore size found over the examined area decreased

from 11.8 to 8.6 μm . This indicates that the porosity was decreased due to a decrease in the amount and size of pores. The average densities of -325 HSPT and -400

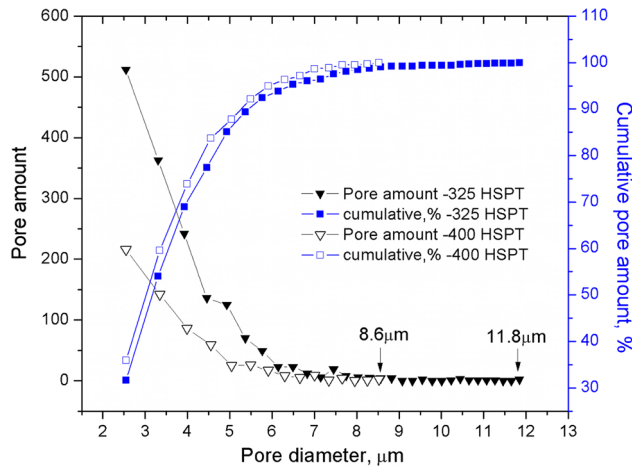


Fig. 4—Pore size distributions in -325 HSPT and -400 HSPT Ti-6Al-4V alloys.

HSPT samples were determined to be 98.53 and 99.23 pct, respectively, using the Archimedes' principle. The porosity decreased by 0.7 pct using a finer starting powder (-400 mesh) and increasing the sintering time to 8 hours.

The microstructural characteristics of HSPT-processed Ti-6Al-4V alloy include, most importantly, a fine $\alpha + \beta$ Widmanstätten microstructure, a relatively thin grain boundary α (GB- α) at prior- β grain boundaries, and some residual sintering pores. The orientation imaging microscopy (OIM) of the microstructure is shown in Figure 5. The orientation map indicates the lack of alignment of the α platelets, in contrast to the colony microstructure with parallel α plates, which typically results from vacuum sintering.^[3,6] The average length and width of the α grains in the microstructure were 2 to 5 and ~ 10 μm , respectively. A coarse- α phase region is shown in Figure 5(c), which was observed in all the three alloys, this coarse- α phase can be a GB α plate or a large α grain adjacent to the prior- β grain boundary. The only microstructural difference between the as-HSPT-processed and HSPT + PIF-processed specimens is the porosity. Since the PIF procedure was

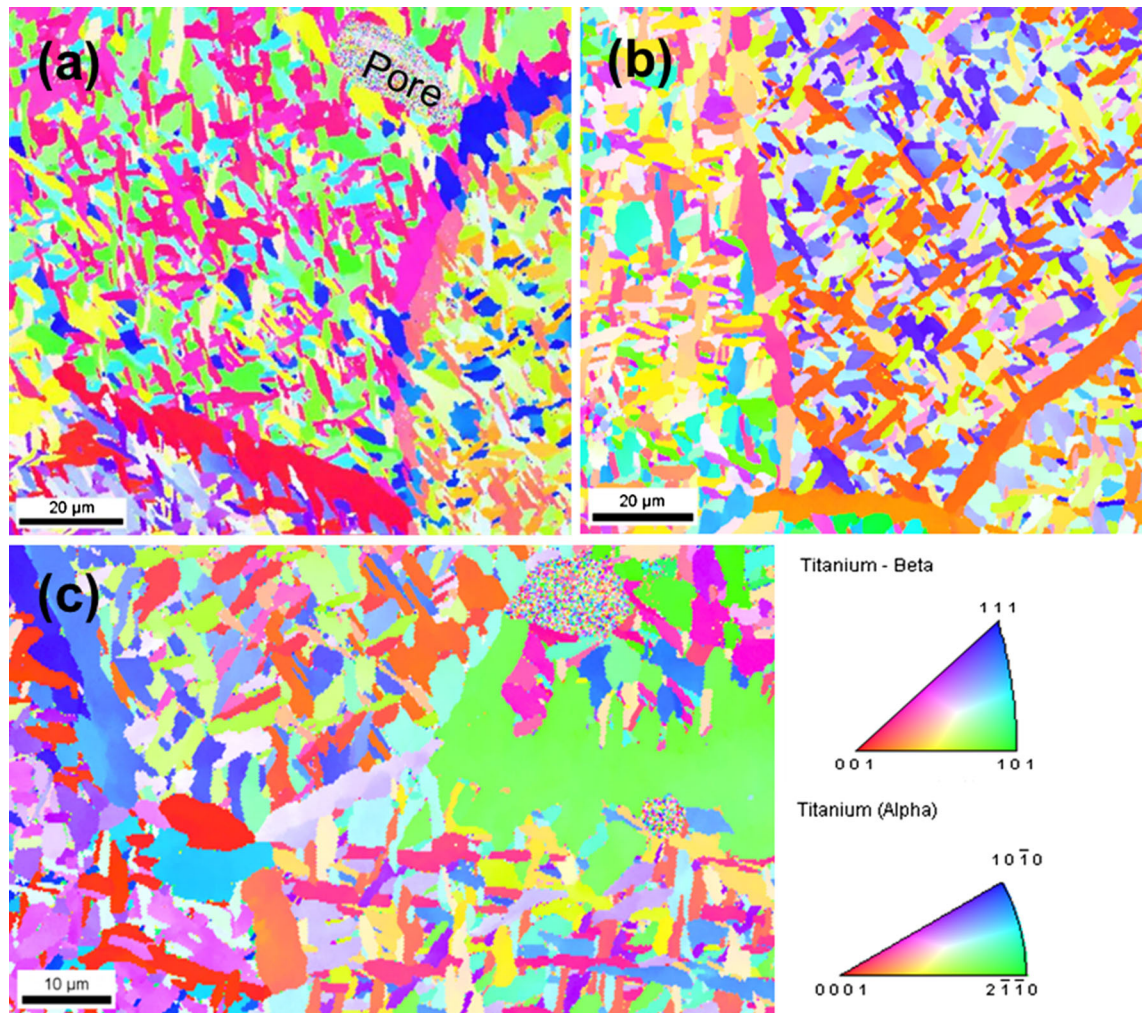


Fig. 5—Orientation imaging microscopies of Ti-6Al-4V alloys: (a) -400 HSPT, (b) -400 HSPT + PIF, (c) and -400 HSPT, which shows a coarse- α phase region (Color figure online).

done at 1123 K (850 °C), which is below the β transus of the Ti-6Al-4V alloy, in a short time, the microstructure did not exhibit any coarsening after the PIF treatment.

B. Tensile Properties

The stress–strain curves for the materials investigated are shown in Figure 6. The average tensile properties are summarized in Table II. At comparable densities, the tensile and yield strengths of the present sintered samples are ~100 MPa higher than those found in the Ti-6Al-4V alloys prepared by other BE PM methods.^[1,2,17] The tensile ductility is either comparable or higher than that obtained in other BE PM methods.^[1,2,17] In the PIFed state, the tensile and yield strengths are also ~100 MPa higher than those of the hot-isostatic-pressed (HIPed) materials prepared by other BE approaches.^[3,7,17] The elongation of the PIFed material here is about 18 pct which is higher than the elongations (12 to 16 pct) obtained in HIPed BE PM Ti-6Al-4V alloys.^[3,7,18] Additionally, the yield and tensile strengths are also approximately 10 pct higher than those for annealed wrought Ti-6Al-4V alloys. The superior tensile properties, at least with respect to the wrought alloy, can be attributed to the fine $\alpha + \beta$ microstructure. Some of the increase in yield and tensile strength may come from the slightly higher oxygen content (0.23 wt pct) compared to that in wrought Ti-6Al-4V (0.2 wt pct) alloy. However, the average ductility for the –400 HSPT + PIF material is about the same as that for an annealed wrought Ti-6Al-4V alloy. This suggests that the effect of microstructure refinement on tensile properties far outweighs any degradation in ductility due to the slightly higher oxygen content.

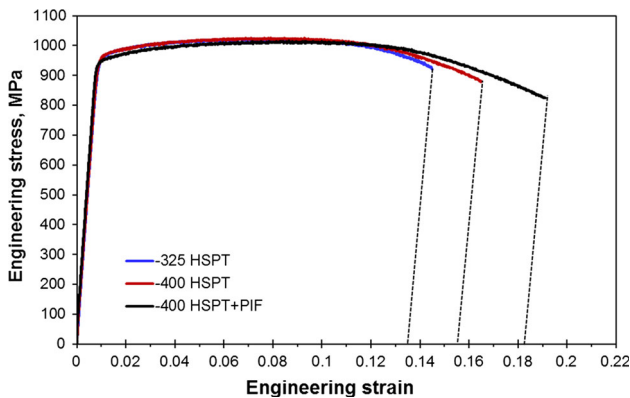


Fig. 6—Stress–strain curves of HSPT-processed Ti-6Al-4V alloys (Color figure online).

C. Fatigue Performance

Figure 7 shows the S-N fatigue data of the Ti-6Al-4V alloys prepared in this study. The fatigue data of wrought Ti-6Al-4V alloy are also included for the purpose of fatigue performance comparison. The HSPT-processed alloys have nearly the same microstructure (Figure 3), though their porosity levels are different. Since the data in Table II affirm that their tensile strengths are almost the same, any difference in their fatigue performance can be attributed only to the differences in porosity.

Fatigue strength here is defined as the maximum stress in the fatigue cycle for which the specimen survived for 10^7 cycles. The fatigue limit strength for the base alloy (–325 HSPT) is around 400 MPa (Figure 7) which is near the low end of the fatigue strength range found in wrought Ti-6Al-4V.^[9] The –400 HSPT samples with less porosity showed a noticeable improvement in fatigue performance, with a fatigue limit of approximately 500 MPa. The improvement was more clearly evident when the data were examined at the stress levels between 500 and 550 MPa. At this stress range, the average fatigue life of –325 HSPT samples was of the order of 10^5 cycles, whereas it was between 10^6 and 10^7 for –400 HSPT samples. This improvement in fatigue performance can be attributed to the relative reduction in porosity, especially the largest pore size. The low-to-intermediate cycle fatigue performance of –400 HSPT + PIF samples was significantly higher than that of the –400 HSPT samples, which is comparable to that of wrought Ti-6Al-4V. This large improvement was mainly due to the elimination of porosity by

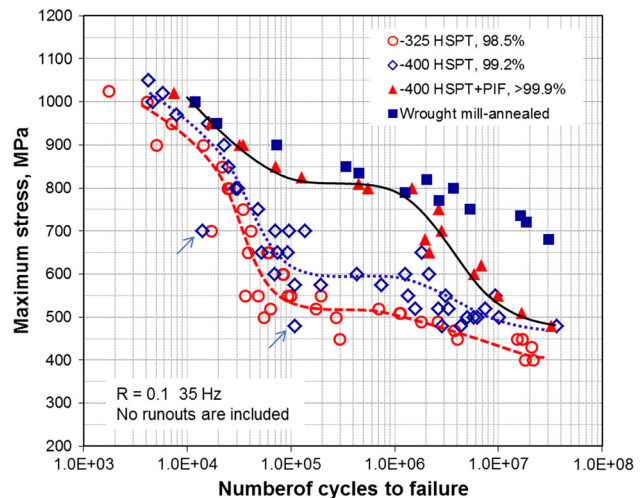


Fig. 7—S-N curves of –325 HSPT, –400 HSPT, –400 HSPT + PIF, and wrought mill-annealed Ti-6Al-4V alloys.

Table II. Tensile Properties of HSPT-Processed Ti-6Al-4V Alloys

Specimen	Sintering Time (h)	Density (pct)	YS (MPa)	UTS (MPa)	EL pct	RA pct
–325 HSPT(6)	4	98.53 (± 0.04)	955 (± 5)	1033 (± 4)	13.7 (± 0.2)	26.0 (± 1.4)
–400 HSPT(6)	8	99.23 (± 0.05)	946 (± 6)	1032 (± 3)	15.6 (± 0.1)	31.6 (± 1.8)
–400 HSPT + PIF(3)	4	>99.9	952 (± 2)	1023 (± 6)	18.2 (± 0.1)	42.1 (± 0.3)

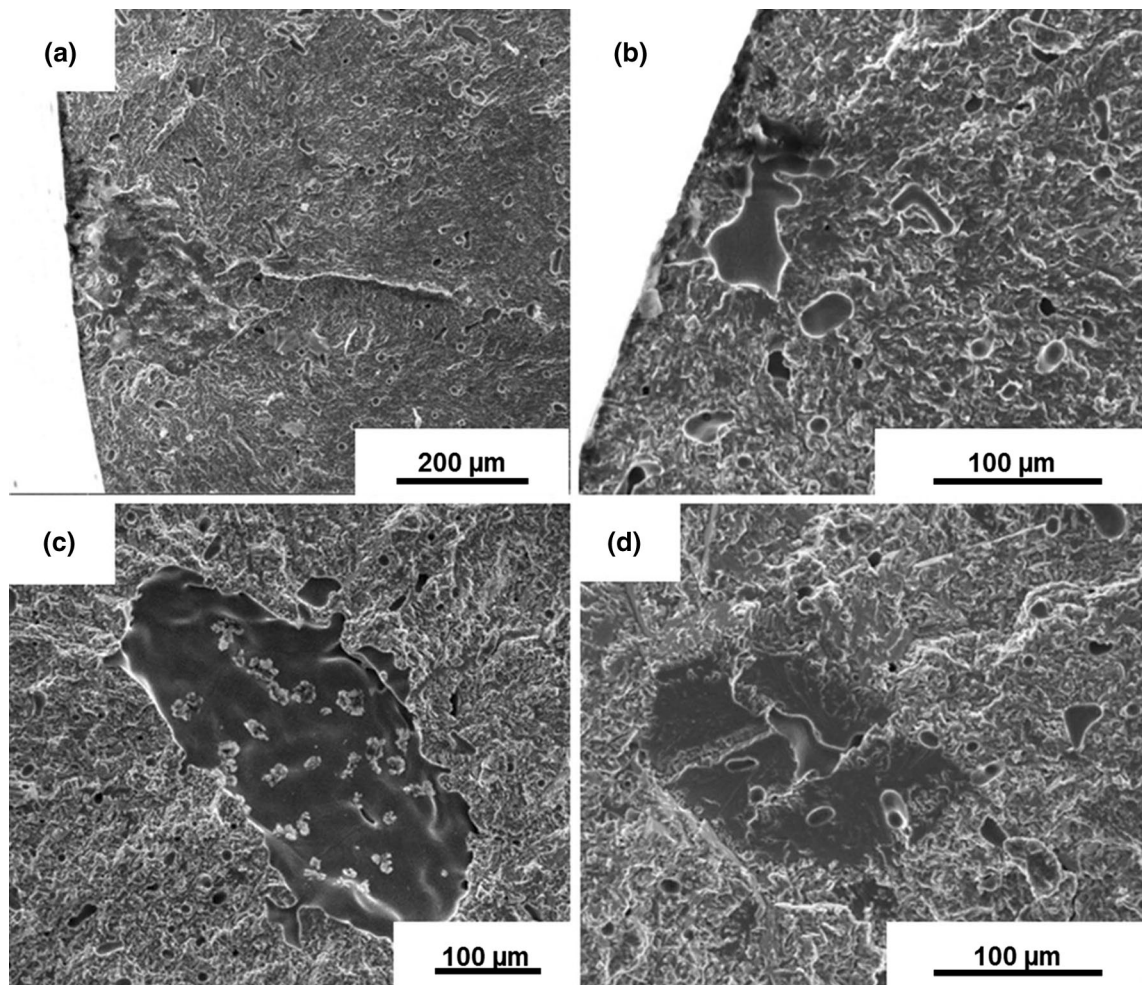


Fig. 8—Fractography of fatigue fractures of -325 HSPT samples. Fatigue cracks initiated from (a) extremely large pore on the surface ($\sigma_{\max} = 450$ MPa, $N_f = 72,666$ cycles), (b) pore cluster near surface ($\sigma_{\max} = 520$ MPa, $N_f = 171,492$ cycles), (c) extremely large pore under surface ($\sigma_{\max} = 400$ MPa, $N_f = 21,341,043$ cycles), and (d) facet with pore cluster ($\sigma_{\max} = 450$ MPa, $N_f = 16,764,731$ cycles).

PIF. However, the HCF performance is still inferior to that of wrought alloy, as shown in Figure 7, the S-N trend of the -400 HSPT + PIF samples declines with stress and approaches the fatigue lives of -400 HSPT samples. The PIF process appears to be ineffective in improving HCF life on the basis of the present S-N fatigue data. Nevertheless, an overall improvement in fatigue performance was achieved by PIF of the Ti-6Al-4V samples prepared with -400 mesh powders.

D. Mechanisms of Fatigue Failure

Fractography of the fatigue-fractured specimens in SEM showed that the equivalent diameter of the crack initiation sites ranged from approximately 20 to 300 μm . At high stress levels, fatigue cracks initiated from pores located at the specimen surface. At low stress levels, the fatigue crack typically initiated from a large internal microstructural discontinuity, a pore or a coarse- α phase region. It will be shown here that the relative fatigue performance of the three materials can be explained on the basis of the microstructure features that lead to fatigue crack initiation.

Typical fatigue crack initiation sites for -325 HSPT specimens at different stress levels are shown in Figure 8. Figures 8(a) and (b) show the crack initiation sites in the low-cycle fatigue region ($N_f < 5 \times 10^5$ cycles). Figure 8(a) is a statistically extreme case, where the initiation pore is quite large, about 200 μm in equivalent diameter. Specimens with such large crack initiation site consistently showed the shortest fatigue life, especially when the site was located on the surface. An example of the most common crack initiation site at high stress levels, in -325 HSPT specimens, is shown in Figure 8(b). This site is made of a cluster of small pores, each with sizes less than 100 μm . Figures 8(c) and (d) show the crack initiation sites in the high-cycle fatigue region. In this region, fatigue cracks started from either an internal pore (Figure 8(c)), or a facet originating from coarse- α phase region containing a cluster of small pores, as shown in Figure 8(d). It is thus clear that the fatigue failures transition from surface crack initiations to internal crack initiations as the cyclic stress is lowered. The flat region in the S-N curve between 10^5 and 10^6 cycles in Figure 7 corresponds to the transition from a surface-initiated to internally initiated fatigue failure mode.

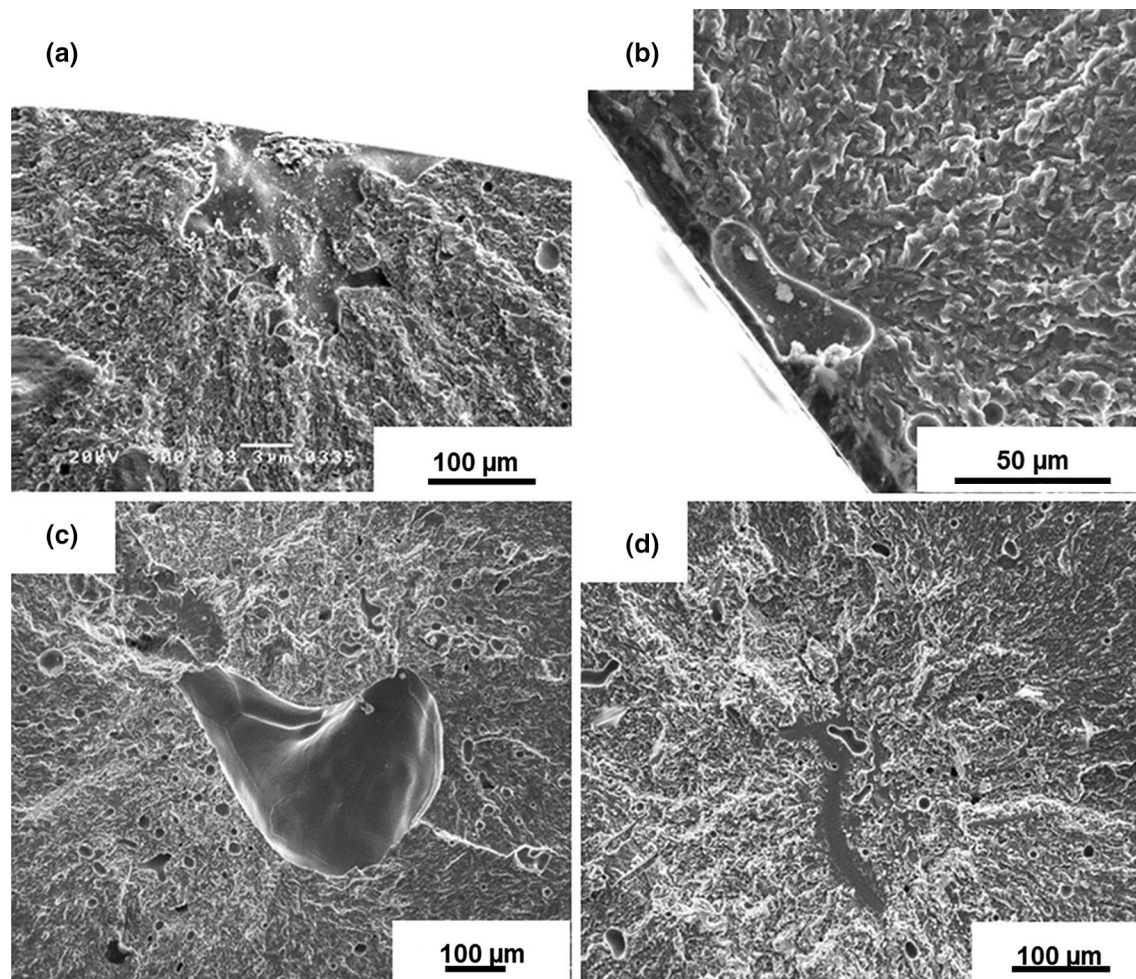


Fig. 9—Fractography of fatigue fractures of -400 HSPT samples. Fatigue cracks initiated from (a) extremely large pore on the surface ($\sigma_{\max} = 480$ MPa, $N_f = 109,423$ cycles), (b) single small pore on the surface ($\sigma_{\max} = 600$ MPa, $N_f = 69,788$ cycles), (c) large pore under surface ($\sigma_{\max} = 520$ MPa, $N_f = 7,469,674$ cycles), and (d) facet under surface ($\sigma_{\max} = 550$ MPa, $N_f = 9,374,617$ cycles).

Fractography of crack initiation sites in the -400 HSPT samples is shown in Figure 9. This sample also exhibited four different types of crack initiations depending on the fatigue stress level, that is, either from extreme-sized ($>100 \mu\text{m}$) pores on the surface (Figure 9(a)), or from small-sized pores on the surface (Figure 9(b)), or from internal pores (Figure 9(c)), or from coarse- α phase regions (Figure 9(d)). However, most initiations were from a relatively smaller single pore, which is in contrast to that observed in -325 HSPT specimens. In Figure 7, the two specimens, indicated by arrows, failed due to the extreme-sized pores on the specimen surface. With the exception of these two data points, the overall fatigue performance of -400 HSPT samples is much improved compared to that of -325 HSPT samples, due to a reduction in overall porosity and the elimination of pore clusters. The -400 HSPT samples also showed the transition from surface-initiated fatigue failures to internally initiated fatigue failures, between 10^5 and 10^6 cycles, similar to that observed in -325 HSPT samples.

Figure 10 shows the fractography of fatigue crack initiation sites for -400 HSPT + PIF specimens at

different stress levels. Figure 10(a) is a typical crack initiation site at $\sigma_{\max} = 900$ MPa—neither pores nor inclusions were seen at the initiation site. They are similar to the crack initiation sites in high stress fatigue failures in wrought materials.^[19] Figure 10(b) shows a crack initiation site near the surface, for $\sigma_{\max} = 700$ MPa, which is made of a set of crystallographic facets. These crack initiation facets are thought to correspond to coarse- α phase regions (see in Figure 5(c)). In one sample, fatigue failure occurred from inclusions, as shown in Figure 10(c). The inclusion was determined to be a foreign particle containing calcium, carbon, and oxygen by EDS point analysis. Figure 10(d) shows a subsurface crack initiation site from facets. This situation is similar to the subsurface crack initiations in wrought Ti-6Al-4V alloys in the very high-cycle fatigue regime ($>10^7$ cycles).^[19–21] Such initiation sites are usually composed of small facets, each with a size equivalent to that of α grains.^[20,21] Regardless, the relatively larger fatigue crack initiation facet size, attributed to coarse- α phase regions in the HSPT specimens, reduces the fatigue life in HCF regime. Coarse- α phase region has longer slip length, which

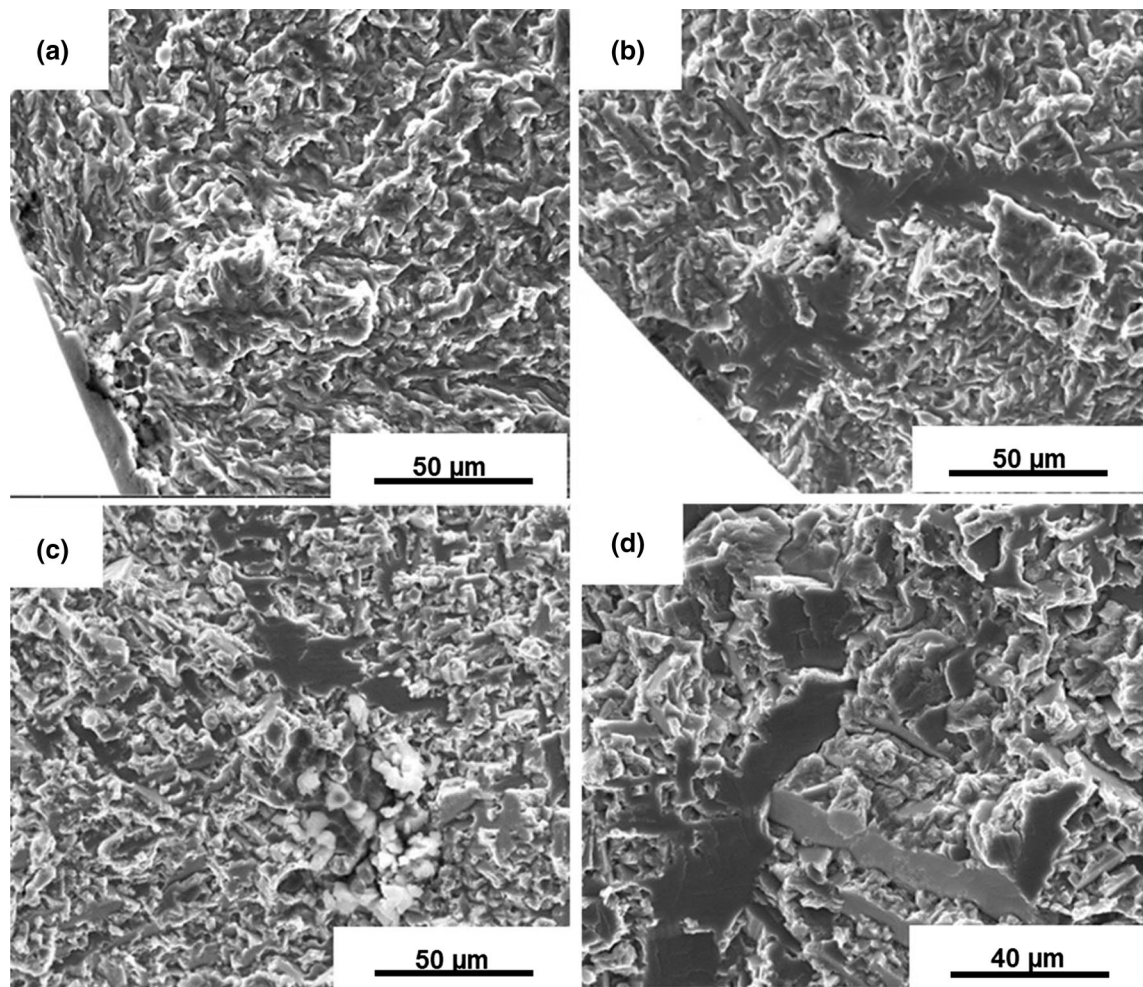


Fig. 10—Fractography of fatigue fractures of -400 HSPT + PIF samples. Fatigue cracks initiated from (a) featureless grain ($\sigma_{\max} = 900$ MPa, $N_f = 32,293$ cycles), (b) facet just below the surface ($\sigma_{\max} = 700$ MPa, $N_f = 2,851,095$ cycles), (c) inclusion together with facet ($\sigma_{\max} = 550$ MPa, $N_f = 9,882,833$ cycles), and (d) facet under surface ($\sigma_{\max} = 510$ MPa, $N_f = 16,945,546$ cycles).

requires a relatively lower stress level to initiate a crack. Thus, the rapid decline of stress at HCF region in the -400 HSPT + PIF samples is due to the ease with which the crack can become critical at lower stress levels to reach the stable crack growth regime.^[22]

It has been found that the role of the PIF processing is to change the crack initiator in fatigue. The only difference between the -400 HSPT specimens and the -400 HSPT + PIF specimens was the porosity, including the extreme-sized pores. The fatigue crack initiation site is determined by the competition between pores and extreme large α phase regions inside the test volume. In fatigue of PM materials, pores usually act as crack initiators and reduce the crack initiation life, and the number of cycles to failure is reduced, compared to pore-free materials.^[23] The total fatigue life is substantively comprised by the crack propagation life, thus any differences in pore size from which the crack would initiate will lead to differences in fatigue life.^[22,24] The -400 HSPT + PIF samples show much improved fatigue performance in the low-to-intermediate cycle fatigue region because of the elimination of pores. The HCF crack initiation sizes in -400 HSPT + PIF

samples are sometimes comparable in size to the crack-initiating pores or coarse- α phase regions in the -400 HSPT samples. When the sizes of crack initiation sites (pores or coarse- α) are similar, the corresponding S-N fatigue lives are also similar, as shown by the overlapped data points in HCF region in Figure 7.

It can be summarized that in the present HSPT-processed PM Ti-6Al-4V alloys, extreme-sized pores or clusters of small pores with a large equivalent size, or coarse- α phase particles when large pores are absent, are the main fatigue crack initiators affecting fatigue life. It is also important to note that sizes of the crack-initiating pores or facets, found on the fracture surfaces, are much larger than the pores/grains typically found on the metallographically polished sections, because these are present in very small numbers. This suggests that fatigue life will be statistical, because the crack initiation and failure life are determined by the chance occurrence of any one of these features in the sample test volume. While a small area metallographic analysis can hardly capture extreme-sized pores or coarse- α phase, a fatigue test will surely capture it by initiating a crack from it, as long as it is present in the test volume. This

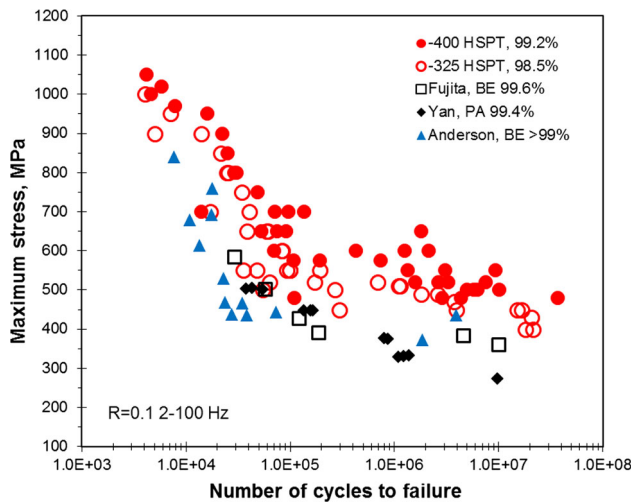


Fig. 11—Comparison of Fatigue performance of Ti-6Al-4V PM alloys prepared by HSPT with the fatigue performance of samples prepared by other PM processes with similar as-sintered density.^[1, 2, 17]

perhaps points to the importance of elimination of extreme-sized pores and α phase regions, in powder metallurgy materials, to obtain a consistent improvement in fatigue performance.

E. Comparison of Fatigue Performance of HSPT Ti-6Al-4V Alloys Against Other PM Ti-6Al-4V Alloys

To put the present study in perspective, S-N fatigue data of PM Ti-6Al-4V alloys from other studies are compared with the present S-N data in Figure 11. The figure shows that the endurance limit stress value (defined at 10^7 cycles) of -400 HSPT samples is about 150 MPa higher than that of other PM-processed materials (the comparison is made at similar sintered density), which have coarse lamellar α colonies in the microstructure.^[1,2,17] This demonstrates the significant advantage of the HSPT process in terms of providing high fatigue strength for the PM Ti-6Al-4V alloy, relative to other PM processes. This improvement can be primarily attributed to the finer $\alpha + \beta$ microstructure resulting from eutectoid phase transformation step in the HSPT process. The hydrogen that was present as hydride in the starting powder facilitated the formation of a finer eutectoid microstructure, when cooled through the β to $\alpha +$ hydride transition temperature, which then led to a finer $\alpha + \beta$ microstructure upon dehydrogenation. Despite the presence of extreme-sized pores in the -400 HSPT samples, they showed a fatigue limit of about 500 MPa, which is very encouraging from the point of view of the potential of the HSPT process for preparing fatigue-resistant titanium components. The fatigue endurance limit can be further improved by eliminating the extreme size pores in this material. This can very likely be achieved with further optimization of TiH_2 powder particle size distribution and HSPT sintering conditions.

Figure 12 shows a comparison of fatigue performance of -400 HSPT + PIF Ti-6Al-4V alloy samples with the results of other works^[3,6,7,25-27] that used HIP and

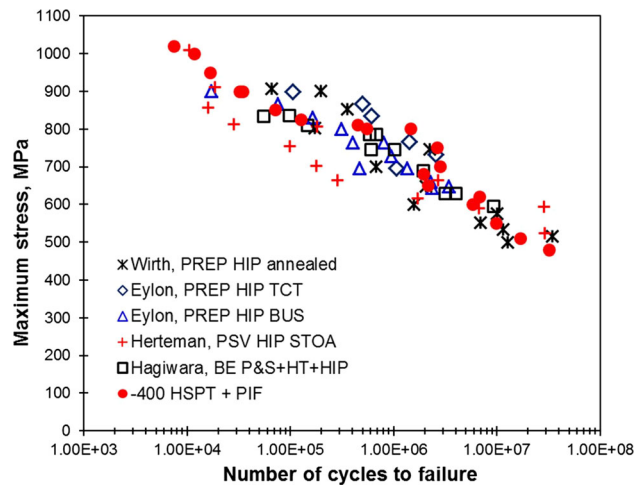


Fig. 12—Comparison of fatigue performance of Ti-6Al-4V alloy prepared by -400 HSPT + PIF process with the fatigue performance of samples prepared by HIP + heat treatment.^[3,6,7,25-27] (TCT, thermochemical treated; BUS, broken-up structure; STOA, solution treated and overaged; P&S, pressed and sintered; HT, heat treated.).

additional heat treatment processes. In general, the HIP and heat treatment steps serve to eliminate porosity and to alter the size, shape, and distribution of α and β phases in the microstructure, thus improving significantly the fatigue performance. It can be seen that the S-N fatigue performance of the present Ti-6Al-4V alloy in the -400 HSPT + PIF condition is quite comparable to the S-N data from other processes, which employed more expensive powders and/or more complicated processing steps. This suggests that the fatigue performance of the materials prepared by the present powder metallurgical approach is at least as good as the best PM Ti-6Al-4V alloys that have been processed through HIP and heat treatment steps. Because the present process uses TiH_2 powder as the raw material, the cost of the present process can be considerably lower than other processes to manufacture PM titanium alloys.

IV. CONCLUSIONS

1. The hydrogen sintering and phase transformation (HSPT) process produces a high-density Ti-6Al-4V alloy with excellent strength, ductility, and good fatigue resistance.
2. The use of -400 mesh TiH_2 powder in sintering resulted in a significant improvement in fatigue performance, relative to -325 mesh powder, due to the increased sintering density and the elimination of pore clusters.
3. When compared at similar density levels, the fine $\alpha + \beta$ microstructure, resulting from the present HSPT process, leads to a significantly improved tensile strength and fatigue performance, relative to the standard powder metallurgical approaches that use blended elements.
4. Fatigue strength in the as-sintered condition is greatly affected by the extreme-sized pores or clusters of pores present in the microstructure,

with the average-sized individual pores generally not participating in any fatigue crack initiation process.

5. Pneumatic isostatic forging (PIF) after sintering closed the residual pores without coarsening the microstructure, which leads to a large increase in fatigue performance. The fatigue performance of HSPT + PIF-processed materials is equivalent to the best fatigue results found in other PM Ti-6Al-4V alloys which were consolidated by HIP followed by additional heat treatment steps.
6. The fatigue crack initiation mechanism in the HSPT-processed Ti-6Al-4V alloy is a competition between the extreme-sized pores and α phase regions. Further improvements in processing with a view to eliminate the extreme-sized crack initiators should lead to even greater improvements in fatigue life of the PM Ti-6Al-4V alloy.

ACKNOWLEDGMENTS

The authors gratefully acknowledge the funding support from the US Department of Energy, Innovative Manufacturing Initiative (DEEE0005761), through the Advanced Manufacturing Office and the Office of Energy Efficiency and Renewable Energy.

REFERENCES

1. T. Fujita, A. Ogawa, C. Ouchi, and H. Tajima: *Mater. Sci. Eng. A*, 1996, vol. 213, pp. 148–53.
2. P.J. Anderson, V.M. Svoyatytsky, F.H. Froes, Y. Mahajan, and D. Eylon: *Modern Develop. Powder Metall.*, 1981, vol. 13, pp. 537–49.
3. D. Eylon, R.G. Vogt, and F.H. Froes: *Modern Develop. Powder Metall.*, 1985, vol. 16, pp. 563–75.
4. Z.Z. Fang, P. Sun, and H. Wang: *Adv. Eng. Mater.*, 2012, vol. 14 (6), pp. 383–87.
5. Z.Z. Fang and P. Sun: *Key Eng. Mater.*, 2012, vol. 520, pp. 15–23.
6. M. Hagiwara and S. Emura: *Mater. Sci. Eng. A*, 2003, vol. 352, pp. 85–92.
7. M. Hagiwara, Y. Kaieda, Y. Kawabe, and S. Miura: *ISIJ Int.*, 1991, vol. 31, pp. 922–90.
8. D. Eylon: *Metall. Trans. A*, 1979, vol. 10A, pp. 311–17.
9. F.H. Froes, S.J. Mashl, V.S. Moxson, J.C. Hebeisen, and V.A. Duz: *JOM*, 2004, vol. 56 (11), pp. 46–48.
10. P. Sun, Z.Z. Fang, and M. Koopman: *Adv. Eng. Mater.*, 2013, vol. 15 (10), pp. 1007–13.
11. P. Sun, Z.Z. Fang, M. Koopman, J. Paramore, K.S. Ravi Chandran, Y. Ren, and J. Lu: *Acta Mater.*, 2015, vol. 84, pp. 29–41.
12. P. Sun, Z.Z. Fang, M. Koopman, Y. Xia, J. Paramore, K.S. Ravi Chandran, Y. Ren, and J. Lu: *Metall. Mater. Trans. A*, 2015, vol. 46A, pp. 1–15.
13. W.R. Kerr, P.R. Smith, M.E. Rosenblum, F.J. Gurney, Y.R. Mahajan, and L.R. Bidwell: *Titanium '80, Science and Technology, Proceedings of the 4th International Conference on Titanium.*, Metall. Soc. of AIME, Kyoto, Japan, 1980, pp. 2477–86.
14. W.R. Kerr: *Metall. Mater. Trans. A*, 1985, vol. 16A, pp. 1077–87.
15. J. Qazi, J. Rahim, F. Froes, O. Senkov, and A. Genc: *Metall. Mater. Trans. A*, 2001, vol. 32A, pp. 2453–63.
16. D.H. Kohn and P. Ducheyne: *J. Mater. Sci.*, 1991, vol. 26, pp. 534–44.
17. Y. Yan, G.L. Nash, and P. Nash: *Int. J. Fatigue*, 2013, vol. 55, pp. 81–91.
18. V.S. Moxson, P. Sjoblom, and M.J. Trzcinski: *Adv. Powder Metall.*, 1992, vol. 6, pp. 125–40.
19. A. Atrens, W. Hoffelner, T.W. Duerig, and J.E. Allison: *Scripta Metall.*, 1983, vol. 17, pp. 601–06.
20. Y. Furuya and E. Takeuchi: *Mater. Sci. Eng. A*, 2014, vol. 598, pp. 135–40.
21. X. Liu, C. Sun, and Y. Hong: *Mater. Sci. Eng. A*, 2015, vol. 622, pp. 228–35.
22. K.J. Miller: *Mater. Sci. Tech.*, 1993, vol. 9, pp. 453–62.
23. A. De Bussac: *Fatigue Fract. Eng. Mater. Struct.*, 1994, vol. 17, pp. 1319–25.
24. F. Cao, P. Kumar, M. Koopman, C. Lin, Z.Z. Fang, and K.S. Ravi Chandran: *Mater. Sci. Eng. A*, 2015, vol. 630, pp. 139–45.
25. J.P. Herteman, D. Eylon, and F.H. Froes: *Powder Metall. Int.*, 1985, vol. 17, pp. 116–19.
26. F.H. Froes, D. Eylon, and S.W. Schwenker: *Progress Powder Metall.*, 1986, vol. 41, pp. 519–30.
27. G. Wirth, K.J. Grundhoff, and W. Smarsly: *S.A.M.P.E Q.*, 1986, vol. 17, pp. 34–39.